Nonaxisymmetric and Axisymmetric Convection in Propagating Reaction-Diffusion Fronts

ARTICLE *in* THE JOURNAL OF PHYSICAL CHEMISTRY · JUNE 1994

Impact Factor: 2.78 · DOI: 10.1021/j100077a014

Nonaxisymmetric and Axisymmetric Convection in Propagating Reaction–Diffusion Fronts

Jonathan Masere,[†] Desiderio A. Vasquez,[‡,⊥] Boyd F. Edwards,[‡] Joseph W. Wilder,[§] and Kenneth Showalter*[,†]

Departments of Chemistry, Physics, and Mathematics, West Virginia University, Morgantown, West Virginia 26506

Received: October 19, 1993; In Final Form: March 23, 1994[⊗]

Observations of steady nonaxisymmetric chemical wave fronts are reported for upward propagation in iodate–arsenous acid solutions within vertical capillary tubes. These observations confirm a recent prediction of hydrodynamic stability theory that the onset of convection in such fronts should be nonaxisymmetric. The nonaxisymmetric waveform reflects the presence of a single convective roll in the vicinity of the moving front.

Introduction

Understanding convective effects in chemical waves represents an interesting and important challenge. Chemical waves create temperature and concentration gradients which can lead to mass density gradients. In the presence of gravity, these density gradients can destabilize planar reaction–diffusion waves, leading to fluid convection and the development of curved fronts. This convection is the source of differences between ascending and descending front propagation speeds in the iron(II)–nitric acid reaction,[1,2] the chlorite–thiosulfate reaction,[2] and the iodate–arsenous acid reaction[3,4] in vertical capillary tubes. Measurements of front speed provide simple tests of proposed reaction–diffusion mechanisms;[5,6] hence, it is important to know when convection contributes to the speed of propagation. Furthermore, it is of interest to understand and predict the effects of convection on the waveform of the propagating front.

Previous experiments on iodate–arsenous acid mixtures[3,4] revealed steady, curved fronts and an increase in propagation speed with increasing tube diameter for ascending waves. The iodate–arsenous acid reaction produces a reacted solution which is less dense than the unreacted solution, so that only upward propagation (with the lighter fluid below) is potentially unstable under the action of gravity. Indeed, descending fronts initiated at the top of the tube remain flat and propagate at a speed independent of the tube diameter. For a tube of diameter 0.94 mm, ascending fronts were also flat and had the same speed as descending fronts, indicating the absence of convection. For diameters of 1.8 mm and above, axisymmetric curved fronts were observed with an approximately parabolic profile and the highest point in the center of the cylindrical tube. The curvature of the ascending fronts increased with increasing tube diameter as did the speed. This curvature was attributed to convection driven by the buoyancy of the reacted fluid, with fluid moving up near the center of the cylinder and down near the cylinder walls.

A theory was recently developed to understand the onset of convection in chemical waves[7–10] and, in particular, to understand the experiments on the iodate–arsenous acid reaction in vertical cylinders. Previous work by Pojman et al.[4,11–13] explained the presence of convection in chemical waves by referring to hydrodynamic results for free convection. In contrast, our theory treats the reaction front explicitly as a thin boundary that separates two different fluids as it propagates within the cylinder. This is possible because the thickness of the region in which the chemical reaction takes place is small compared with all other length scales in the problem. Our thin-front results[7,9] compare favorably with our more complete calculations involving the reaction–diffusion equation for the system.[10] The linear stability analysis[9] predicts a nonaxisymmetric front near the onset of convection in vertical cylinders, with fluid rising in half of the cylinder and falling in the other half, as shown in Figure 1. The predicted highest point of the front is not in the center as was observed in the previous experiments. This apparent discrepancy led us to make new measurements closer to the onset of convection. In this paper, we report the results of these experiments and review the theory that motivated them.

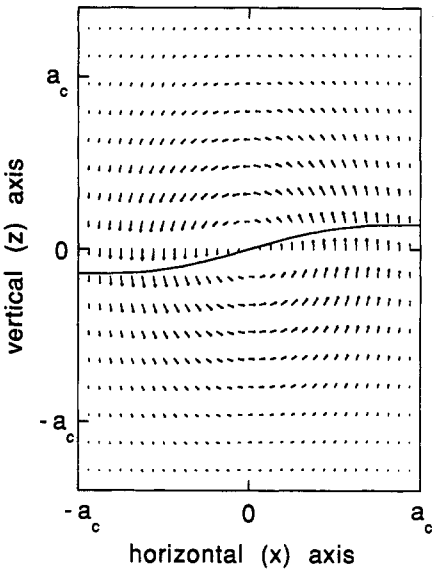

Figure 1. Velocity field for the predicted nonaxisymmetric mode at the onset of convection. A cross section through the axis of a vertical cylinder of radius a is shown. The solid line represents the interface between the unreacted solution above and the lighter reacted solution below. Although the fluid velocity vectors in this figure are those shown in Figure 2 of ref 9, the solid line depicting the front has been corrected to reflect the appropriate boundary conditions.

Theory

In the absence of convection, the fronts observed in the iodate–arsenous acid reaction have been modeled successfully using a one-variable reaction–diffusion equation.[5,6] To understand the convective effects on the fronts, we couple this model with hydrodynamics. The resulting model[10] is made up of the reaction–

* To whom correspondence should be addressed.
† Department of Chemistry.
‡ Department of Physics.
§ Department of Mathematics.
⊥ Current address: Department of Physics, Indiana University–Purdue University at Fort Wayne, Fort Wayne, IN 46805.
⊗ Abstract published in *Advance ACS Abstracts,* June 1, 1994.

0022-3654/94/2098-6505$04.50/0

diffusion equation and the fluid–dynamic equations of motion:

$$\rho\left[\frac{\partial \mathbf{v}}{\partial t} + (\mathbf{v}\cdot\nabla)\mathbf{v}\right] = -\rho g\hat{z} - \nabla P + \rho\nu\nabla^2\mathbf{v} \quad (1a)$$

$$\nabla\cdot\mathbf{v} = 0 \quad (1b)$$

$$\frac{\partial c}{\partial t} + \mathbf{v}\cdot\nabla c = D\nabla^2 c + f(c) \quad (1c)$$

Here, $\mathbf{v}$ is the fluid velocity, P is the pressure, ν is the kinematic viscosity, c is the iodide concentration, D is the molecular diffusivity, g is the acceleration due to gravity, ρ is the fluid density, and $f(c)$ is the reaction term; for the iodate–arsenous acid reaction $f(c)$ is a third-order polynomial. The first two equations express force balance and mass continuity. The third equation describes molecular diffusion in the presence of fluid flow. Although the reaction is slightly exothermic and the overall density differences due to thermal expansion and chemical composition are comparable, we do not include a heat diffusion equation here. This is justifiable because the length scale for temperature variations is large compared with the convective length scale, so that the thermally induced density changes are negligible within the convective region of interest.[14]

The convectionless solution, where a flat front unbounded in the horizontal direction propagates vertically with constant speed, satisfies this set of equations. Ascending flat fronts are unstable to perturbations of horizontal wavelength greater than a critical wavelength.[10] Thus, perturbations grow when the diameter of the tube is greater than this critical wavelength, while they decay if the diameter is smaller. This result provides a qualitative explanation of why the upward front is stable for small diameters, since then the cylinder diameter is smaller than the critical wavelength. It was also shown that the results based on this model are well approximated by a thin-front model in which the reaction–diffusion equation is replaced by the eikonal relation[7,10]

$$C - \hat{n}\cdot\mathbf{v}|_f = C_0 + D\kappa \quad (2)$$

Here, C is the normal velocity of the front, C_0 is the flat front speed, $\mathbf{v}|_f$ is the fluid velocity at the reaction front, κ is the curvature of the front, and $\hat{n}$ is a unit vector perpendicular to the front pointing into the unreacted fluid. The second term on the left-hand side was added to the standard eikonal equation[15] to allow for fluid flow.[7,16] This term accounts for the speed of the front in the normal direction due to the flow of the underlying fluid. The eikonal relation provides a stability mechanism for the propagating fronts, since it tends to lower the hills (negative curvature, lower normal speed) and raise the valleys (positive curvature, higher normal speed). It is the interplay between this stabilizing force and the destabilizing force of fluid buoyancy that allows a stable nonplanar front. Such propagating fronts occur when these two forces are exactly balanced. Under conditions such that the stabilizing forces are dominant, the front remains flat. When the forces due to buoyancy dominate, the system may exhibit more complex behavior such as plumes.

In the calculations presented here, we impose no-slip and no-normal-flow boundary conditions at the cylinder walls. After transforming eqs 1 into a dimensionless form, it is found that there is only one parameter that determines the convective stability of planar ascending fronts in vertical cylinders. This dimensionless driving parameter,[9]

$$\mathcal{S} = \delta g a^3/\nu D \quad (3)$$

involves the cylinder radius a and the fractional density difference $\delta = (\rho_u - \rho_r)/\rho_r$ between the unreacted fluid density (ρ_u) and the reacted fluid density (ρ_r). The parameter measures the strength of buoyancy, which tends to destabilize a flat front in favor of convection, as opposed to curvature effects which tend to flatten the front. The parameter $\mathcal{S}$ is directly relevant to convection in autocatalytic systems, since it includes a reaction front and localized density gradients. Linear calculations[9] using this theory predict that planar ascending fronts are unstable to nonaxisymmetric convection for $\mathcal{S} > \mathcal{S}_c = 87.9$ and to axisymmetric convection for $\mathcal{S} > \mathcal{S}_{c2} = 370.2$. The nonaxisymmetric convection is therefore predicted to appear at the onset of convection. It consists of a single convective roll in the vicinity of the moving front, with upflow on one side of the cylinder and downflow on the other, and a peak and a valley in the front surface in the corresponding halves of the cylinder. Thus, changing the cylinder radius or the density difference can take the system through the convective threshold at $\mathcal{S} = \mathcal{S}_c$. The earlier experiments[3,4] were performed for $\mathcal{S} = 48$ and $\mathcal{S} \geq 337$, which correspond to the inside diameters $d = 0.94$ mm and $d \geq 1.8$ mm discussed in the Introduction. The experiments reported here were carried out to better locate the onset of convection.

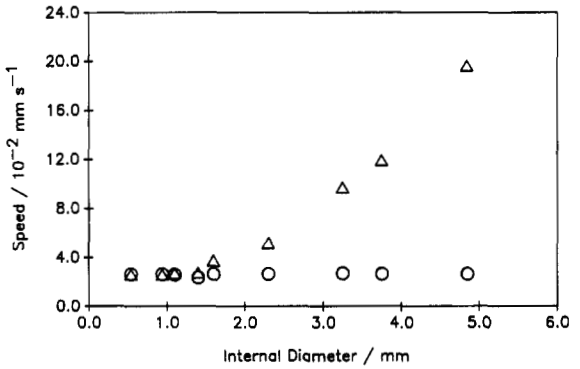

Figure 2. Measured front speeds as a function of tube diameter. Circles and triangles represent descending and ascending fronts, respectively. For tube diameters equal to and below 1.1 mm, the ascending speed is the same as the descending speed. For larger diameters, convection enhances the speed of the ascending fronts. Initial reactant concentrations and conditions are $[IO_3^-] = 5.0 \times 10^{-3}$ M, $[H_3AsO_3] = 3.0 \times 10^{-2}$ M, pH = 2.255, and $T = 25.0 \times 0.1$ °C.

Experiments

Reaction mixtures were prepared from reagent-grade chemicals and distilled water. Initial concentrations were determined by pipetting appropriate volumes of KIO_3, H_3AsO_3, buffer ($NaHSO_4/Na_2SO_4$), and starch stock solutions. Wave propagation experiments were carried out using water-jacketed capillary tubes thermostated at 25.0 ± 0.1 °C. Waves were electrochemically initiated at a negatively biased Pt electrode, and wave front position as a function of time was measured visually using a millimeter scale attached to the capillary or with a digital imaging system. Details of the experimental procedure are given in refs 3 and 4. A description of the imaging analysis is given in ref 17.

The first set of experiments was carried out using a series of tubes of different internal diameters containing reaction mixtures of the same composition. In this way, the driving parameter $\mathcal{S}$ changes as the cylinder radius a is varied. These experiments are similar to the ones previously reported in refs 3 and 4 except here we have used more tubes to increase the range and resolution of a. The remaining experimental quantities that determine $\mathcal{S}$ are the fractional density difference $\delta = 1.74 \times 10^{-2}\ M^{-1}[IO_3^-]$ (from earlier measurements[3,4]), the viscosity $\nu = 9.2 \times 10^{-3}$ cm^2 s^{-1}, the molecular diffusivity $D = 2.0 \times 10^{-5}$ cm^2 s^{-1}, and the acceleration of gravity $g = 980$ cm s^{-2}. The results of the experiments are summarized in Figure 2. For experiments carried out with tubes of internal diameter equal to or smaller than 1.1 mm, the velocity of the ascending fronts matches the velocity of the descending fronts. These fronts are flat, although, as shown in Figure 3a, there is evidence of a slight amount of convection for a tube of 1.1-mm i.d. For cylinders of 1.4-mm i.d. and larger, the speed of the ascending fronts is clearly higher than the speed of the descending fronts. The speed of the ascending fronts increases

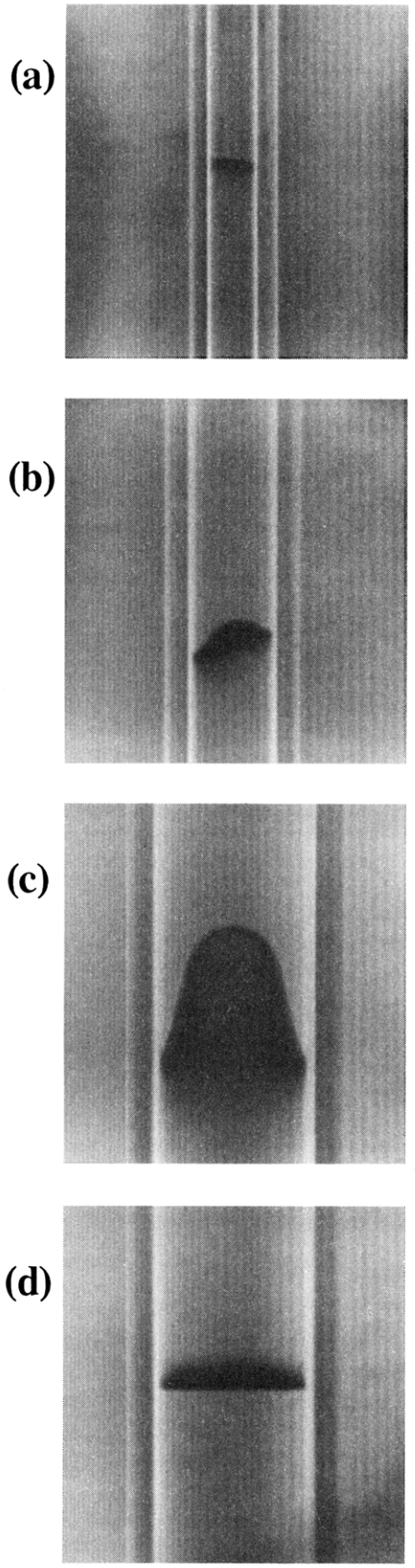

Figure 3. Waveforms of ascending and descending iodate–arsenous acid fronts in a vertical cylinder. The ascending front is (a) flat, (b) nonaxisymmetric, and (c) axisymmetric for tube internal diameters of 1.1, 1.6, and 3.2 mm, respectively; (d) example of flat descending front, shown for an internal diameter of 3.2 mm. Reactant concentrations and conditions are the same as Figure 2.

as the tube diameter is increased above this diameter, while the speed of the descending fronts is independent of the diameter.

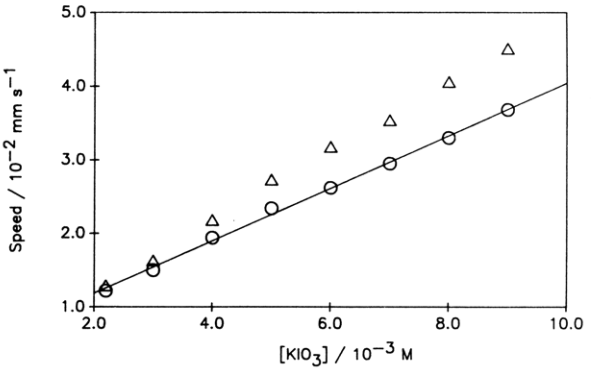

Figure 4. Speed of ascending (triangles) and descending (circles) fronts with different iodate concentrations in a 1.4-mm-i.d. tube. Initial reactant concentrations and conditions are $[IO_3^-] = (2.2–9.0) \times 10^{-3}$ M, $[H_3AsO_3] = 3.0 \times 10^{-2}$ M, pH = 2.255, and $T = 25.0 \pm 0.1$ °C.

The increased speed and the front curvature (Figure 3b,c) are due to convection induced by the presence of heavy unreacted fluid above the lighter reacted fluid. For cylinders of 0.9-mm i.d. and smaller, there is clearly no convection.

These new measurements allow a direct comparison with the theory. On the basis of the observations of the front speed in Figure 2, we estimate the critical diameter for the onset of convection to be 1.1 ± 0.1 mm. The uncertainty arises in locating where the ascending and descending front speeds separate. This corresponds to an experimental critical driving parameter of $\mathcal{S}_c = 77 \pm 21$, which clearly agrees with the theoretical value $\mathcal{S}_c = 87.9$ for the onset of nonaxisymmetric convection.

Convection is also responsible for modifying the shape of the ascending fronts. A nonaxisymmetric ascending front near the onset of convection is shown in Figure 3b. This observation confirms the theoretical prediction that the onset should be nonaxisymmetric. The front is higher on one side of the tube, as predicted by the theory (cf. Figure 1). The nonaxisymmetric convective state is observed in tubes of internal diameters 1.4 mm ($\mathcal{S} = 158.9$) and 1.6 mm ($\mathcal{S} = 237.2$), whereas an axisymmetric state (Figure 3c) is observed for tubes of internal diameters 2.3 mm ($\mathcal{S} = 704.7$) and above. Thus, we observe an experimental transition from nonaxisymmetric convection to axisymmetric convection between $\mathcal{S} = 237.2$ and $\mathcal{S} = 704.7$. Curiously, the predicted threshold of instability $\mathcal{S}_{c2} = 370.2$ of a flat front to axisymmetric convection lies between these experimental values. However, theoretical proof of such a transition will require an analysis of the stability of steady nonaxisymmetric convection.

Experiments were also carried out in which the iodate concentration was varied in the reaction mixture. Changes in $[IO_3^-]$ result in a proportional change in the fractional density difference[7] and, in turn, the driving parameter $\mathcal{S}$. There is, however, a much smaller variation of $\mathcal{S}$ with $[IO_3^-]$ compared to the cubic dependence on tube radius. The results of experiments carried out using a 1.4-mm i.d. tube are shown in Figure 4, where the speeds of ascending and descending fronts are plotted as a function of the iodate concentration. Waves could not be monitored at IO_3^- concentrations below 2.2×10^{-3} M, since the concentration of I_3^- becomes too small to visualize the front with our imaging system. All of the convective fronts in this set of experiments were nonaxisymmetric, while the convectionless fronts of the descending waves were flat. The largest value of $\mathcal{S}$ in these experiments is 279.5.

The speed of convectionless descending fronts varies linearly with the iodate concentration in Figure 4, as predicted by reaction–diffusion theory.[5,6] The velocity from an analytical solution of the reaction–diffusion equation is given by

$$C = m + n[IO_3^-]_0 \qquad (4)$$

where $m = k_1(2D/k_2)^{1/2}[H^+]_0 = 7.45 \times 10^{-5}$ mm s^{-1}, $n = (k_2D/$

$2)^{1/2} = 3.73$ mm s^{-1} M^{-1}, $[H^+]_0 = 5.56 \times 10^{-3}$ M, $D = 2.0 \times 10^{-5}$ cm^2 s^{-1}, and the rate constants for the iodate–arsenous acid reaction[18] are $k_1 = 4.5 \times 10^3$ M^{-3} s^{-1} and $k_2 = 4.5 \times 10^8$ M^{-4} s^{-1}. The reaction–diffusion wave velocity is almost completely determined by the second term in eq 4, as the first term contributes less than 1% to the velocity over the range of $[IO_3^-]$ in Figure 4. The values of the parameters predicted from reaction–diffusion theory compare with $m = 4.69 \times 10^{-3}$ mm s^{-1} and $n = 3.57$ mm s^{-1} M^{-1} from the least-squares fit shown in Figure 4. There is good agreement between the measured and predicted velocities for a particular $[IO_3^-]$.

In Figure 4, the ascending wave velocity is greater than the descending wave velocity, with the difference increasing with increasing $[IO_3^-]$ above the experimental limit of 2.2×10^{-3} M. Taking the velocity dependence on $[IO_3^-]$ for the ascending wave as linear near the onset of convection, a least-squares fit to the first four points generates a straight line that intersects the line described by eq 4 at $(2.2 \pm 0.5) \times 10^{-3}$ M. The corresponding experimental determination of the critical driving parameter for the onset of convection, $\mathcal{S}_c = 70 \pm 16$, is just below the theoretical value[7-10] $\mathcal{S}_c = 87.9$. Although the ascending and descending speeds differ at 2.2×10^{-3} M, the difference is insignificant compared with the uncertainty in the individual front speeds, which is approximately half the width of the plotting symbols. This series of experiments complements the measurements described above in which the tube diameter was varied.

Conclusions

The experiments reported here verify an earlier theoretical prediction that a nonaxisymmetric front is exhibited near the onset of convection. The experiments also show that no convection occurs in ascending fronts for values of $\mathcal{S}$ smaller than a critical value $\mathcal{S}_c$. For values of $\mathcal{S}$ slightly above the onset of convection, the front is observed to be nonaxisymmetric, while for higher $\mathcal{S}$ the front is axisymmetric. The experimental threshold value $\mathcal{S}_c = 77 \pm 21$ obtained by varying the tube diameter agrees with the theoretical value $\mathcal{S}_c = 87.9$. The experimental value $\mathcal{S}_c = 70 \pm 16$ obtained by varying the iodate concentration is slightly below this theoretical value. The uncertainties in these experimental values reflect the uncertainty in locating where the ascending and descending front speeds begin to differ.

The agreement between the measured and predicted values of tube size or iodate concentration for the onset of convection is put into better perspective by an assessment of possible errors. A likely source of systematic error in $\mathcal{S}_c$ is rounding in the front speed near the onset of convection, which would lead to deflated experimental values of $\mathcal{S}_c$. Such rounding, which could arise even from slight tube imperfections, is ubiquitous at transitions such as this one. Uncertainties in the values of the parameters of eq 3 may also play a role. In particular, lacking values of the kinematic viscosity ν for the dilute chemical mixtures of interest, we have used that of pure water. The rather tricky measurement of the very small density difference δ is another possible source of error. Most notably, any errors or nonuniformities in the tube radius a are magnified 3-fold in $\mathcal{S}$ owing to its cubic dependence on a.

The assessment of the experimental uncertainties should be balanced by an assessment of the theoretical uncertainties. The theoretical corrections to the critical wavelength for a laterally unbounded system due to the noninfinite thermal diffusivity of the fluid and to the nonzero thickness of the chemical reaction front are <1% and ≈5%, respectively.[10,14] Although these effects may result in corresponding 3-fold-magnified corrections in the theoretical values of $\mathcal{S}$, an attempt to include these complicating effects in the already complicated cylindrical geometry has not yet been made. Including noninfinite thermal diffusivity of the fluid would raise the issue of the appropriate thermal boundary conditions at the cylinder walls, which might have a nonnegligible effect. The full resolution of these issues awaits further investigation.

In view of these uncertainties and that there are no adjustable parameters in the treatment, the agreement between the experimental and theoretical values of $\mathcal{S}_c$ is remarkably good.

Further theoretical work is being pursued to account for the increase of front propagation speed due to convection and to explain the transition from nonaxisymmetric to axisymmetric convection. This requires a nonlinear calculation, either by direct numerical solution of the reaction–diffusion–convection equations or by solving a nonlinear front evolution equation derived from the eikonal relation.

It would be interesting to study the propagation of reaction–diffusion waves in vertical slabs, for which the fluid is confined to the gap between two parallel or nearly parallel plates. For parallel plates, the theory predicts that long-wavelength convection exists even as $\mathcal{S} \to 0$ (ref 19). However, nonparallel plates should preclude such long wavelengths and should therefore allow convection only above a critical value of $\mathcal{S}$. Whether steady periodic patterns can be stabilized in such a system is an open question.

Acknowledgment. We thank Dezső Horváth for taking the photographs of the propagating fronts. This work was supported by the National Science Foundation (Grant CHE-9222616), WV-EPSCoR (RII-8922106 and OSR-9255224), and the National Research Center for Coal and Energy. Acknowledgment is made to the donors of the Petroleum Research Fund, administered by the ACS, for partial support of this research.

References and Notes

(1) Bazsa, G.; Epstein, I. R. *J. Phys. Chem.* **1985**, *89*, 3050.
(2) Nagypál, I.; Bazsa, G.; Epstein, I. R. *J. Am. Chem. Soc.* **1986**, *108*, 3635.
(3) McManus, T. Ph.D. Thesis, West Virginia University, 1989; Chapter 3.
(4) Pojman, J. A.; Epstein, I. R.; McManus, T. J.; Showalter, K. *J. Phys. Chem.* **1991**, *95*, 1299.
(5) Hanna, A.; Saul, A.; Showalter, K. *J. Am. Chem. Soc.* **1982**, *104*, 4848.
(6) Saul, A.; Showalter, K. In *Oscillations and Traveling Waves in Chemical Systems*; Field, R. J., Burger, M., Eds.; Wiley: New York, 1985; p 419.
(7) Edwards, B. F.; Wilder, J. W.; Showalter, K. *Phys. Rev. A* **1991**, *43*, 749.
(8) Vasquez, D. A.; Edwards, B. F.; Wilder, J. W. *Phys. Rev. A* **1991**, *43*, 6694.
(9) Vasquez, D. A.; Wilder, J. W.; Edwards, B. F. *Phys. Fluids A* **1992**, *4*, 2410.
(10) Vasquez, D. A.; Wilder, J. W.; Edwards, B. F. *J. Chem. Phys.* **1993**, *98*, 2138.
(11) Pojman, J. A.; Epstein, I. R. *J. Phys. Chem.* **1990**, *94*, 4966.
(12) Pojman, J. A.; Nagy, I. P.; Epstein, I. R. *J. Phys. Chem.* **1991**, *95*, 1306.
(13) Nagy, I. P.; Pojman, J. A. *J. Phys. Chem.* **1993**, *97*, 3443.
(14) Vasquez, D. A.; Edwards, B. F.; Wilder, J. W. To be published.
(15) Tyson, J. J.; Keener, J. P. *Physica D* **1988**, *32*, 327.
(16) Wilder, J. W.; Vasquez, D. A.; Edwards, B. F. *Phys. Rev. E* **1993**, *47*, 3761.
(17) Winston, D.; Arora, M.; Maselko, J.; Gáspár, V.; Showalter, K. *Nature* **1991**, *351*, 132. A narrow band-pass filter of 500 ± 5 nm was used with an integrating sphere for detection of the starch–I_3^- complex in the wavefront.
(18) Ganapathisubramanian, N.; Reckley, J. S.; Showalter, K. *J. Chem. Phys.* **1989**, *91*, 938.
(19) Huang, J.; Vasquez, D. A.; Edwards, B. F.; Kolodner, P. *Phys. Rev. E* **1993**, *48*, 4378.